Available online at www.sciencedirect.com
SCIENCE DIRECT®
Journal of Sound and Vibration 283 (2005) 853–873
JOURNAL OF SOUND AND VIBRATION
www.elsevier.com/locate/jsvi

A numerical method for the calculation of dynamic response and acoustic radiation from an underwater structure

Q. Zhou[a,*], P.F. Joseph[b]

[a]*Ship Science Department, 339 Jie Fang Road, Wuhan 430033, PR China*
[b]*Institute of Sound and Vibration Research, University of Southampton, Highfield, Southampton, SO17 1BJ, UK*

Received 19 September 2003; received in revised form 25 February 2004; accepted 17 May 2004
Available online 18 November 2004

Abstract

An approach combining finite element with boundary element methods is proposed to calculate the elastic vibration and acoustic field radiated from an underwater structure. The FEM software NASTRAN is employed for computation of the structural vibration. An uncoupled boundary element method, based on the potential decomposition technique, is described to determine the acoustic added mass and damping coefficients that result due to fluid loading effects. The acoustic matrices of added mass and damping coefficients are then added to the structural mass and damping matrices, respectively, by the DMAP modules of NASTRAN. Numerical results are shown to be in good agreement with experimental data. The complex eigenvalue analyses of underwater structure are obtained by NASTRAN solution sequence SOL107. Results obtained from this study suggest that the natural frequencies of underwater structures are only weakly dependent on the acoustic frequency if the acoustic wavelength is roughly twice as large as the maximum structural dimension.

1. Introduction

A recent paper by the authors [1] has described an uncoupled boundary element method (BEM) for determining the acoustic added mass and damping experienced by a vibrating structure in a

*Corresponding author. Institute of Sound and Vibration Research, University of Southampton, Highfield, Southampton SO17 1BJ, UK. Tel.: +44 23 8059 3613; fax: +44 23 8059 3190.
E-mail address: sz@isvr.soton.ac.uk (Q. Zhou).

0022-460X/$ - see front matter © 2004 Elsevier Ltd. All rights reserved.
doi:10.1016/j.jsv.2004.05.028

dense fluid due to fluid-loading effects. Ref. [1] dealt with a simple example of a piston source oscillating on a rigid sphere in which the effects of fluid loading on source vibration did not need to be considered. In this paper, the effect of fluid loading on the structure and its subsequent radiation will be addressed. The method presented in Ref. [1] will be applied to predict the acoustic pressure field radiated by a harmonically excited three-dimensional elastic structure that is either completely submerged in fluid or located on a free surface. The analysis will demonstrate how the eigenvalues of a fluid-coupled structure may be solved using the widely used structural analysis code, NASTRAN, which is normally used to solve structural eigenvalues in vacuum. Knowledge of the eigenvalues of fluid-coupled structures is important since the structural designer must ensure that natural frequencies of structures are not coincident with their excitation frequencies. Ali et al. [2] have reviewed acoustic eigenvalue problems and pointed out that, ''When a structure is submerged in a fluid of infinite extent, e.g. a submarine submerged in sea water, the vibration characteristics of the structure changes dramatically. Although the problem can be addressed by finite element method (FEM), it is far from being efficient, as a large fluid domain needs to be included in the finite element (FE) model in order to solve the problem with a reasonable accuracy. To our knowledge, this problem has not yet been addressed in the context of BEM. Particularly, how to compute an accurate fluid mass matrix in this situation is still an open question that needs be answered''.

The emphasis in this paper is on the numerical prediction of the dynamic response of elastic structures subjected to external fluid loading. The fluid density (typically water) is assumed to be sufficiently high that the effects of coupling between the fluid and structure become important. The approach proposed here will employ a combination of structural FE and fluid boundary element (BE) techniques.

The use of NASTRAN for solving the problems of fluid–structure interactions has several advantages. First it allows the capability of treating complex structures of large scale and also in the computation of their complex eigenvalues, which may be caused by non-symmetric fluid-loading matrices. Second, the Direct Matrix Abstraction Program (DMAP) in NASTRAN enables exterior added mass and damping matrices due to fluid loading effects to be directly inputted into structural mass and damping matrices so that the effects on the structure of fluid loading may be calculated. Furthermore, the DMAP matrix solver can efficiently solve the large, complex, fully populated, non-symmetric system of algebraic equations that arises from BEM. Third, the pre- and postprocessor PATRAN developed for use with NASTRAN not only allows the numerical mesh to be easily created but also enables the vibration modes and the acoustic fields to be visualized easily.

Acoustic wave propagation in the fluid can be modelled using either FE [3–6], infinite elements (IE) [7–10] or BE techniques [11–13]. The comparitive merits of each technique are discussed in review papers by Everstine [15], Astley [10] and Morino [16]. The fluid FEM is ideally suited to solving interior domain problems. For exterior domain problems, the FEM is complicated by the difficulty in specifying the radiation boundary condition at the outer fluid boundary. The simplest radiation boundary condition is the plane wave approximation [14]. A more accurate radiation boundary condition may be imposed by applying the infinite element method (IEM). Typically, in structural radiation problems a small portion of the exterior fluid is modelled with finite elements, outside of which a layer of fluid infinite elements is added. This combined FE and IE method could be used for solving problems with or without mean flow, although it has the advantage of

being able to solve problems involving a non-uniform mean flow where obtaining a Green function is difficult. Fortunately, in most underwater vibroacoustic problems, the flow Mach number is very small and mean flow effects can be ignored. In this case the free-space Green function can be used to establish boundary integral equations on which the BEM is based. Since no fluid-domain element is involved in the numerical calculation, BEM is a more efficient approach than FEM provided that the Green function of the problem can be found. The BEM technique employed in this paper differs from Everstine's BEM approach [13], which directly solves a discrete form of Helmholtz integral equation while in this paper the BEM equations are derived from differential equations through the potential decomposition technique [1]. This potential decomposition technique allows the added mass and damping coefficients due to fluid loading to be obtained *before* the structural dynamic equations are solved. It is this property that allows eigenvalue analysis for fluid-loaded structures to be performed.

In order to solve for the response of a structure submerged in fluid, the fluid loading on the wet interface must be known. Conversely, to obtain the fluid loading on the structure, the structural motion on the wet interface must be determined. A more desirable way of solving the coupled system is to uncouple the systems into two sets of matrix equations and to solve each set of equations separately. Two different procedures have been proposed to do this. One was described by Everstine and Henderson [13]. Another approach will be used in this paper. The solution procedure used by Everstine and Henderson [13] is outlined below:

(i) Invert the structural impedance matrix of structural dynamic equations to establish a matrix equation that relates the velocity V and pressure p on the interface between the fluid and structure (solve structural dynamic equation first).
(ii) Discretize Helmholtz integral equation to obtain another matrix equation between V and p.
(iii) Eliminate the velocity variable V from above two equations to give an equation involving only pressure.
(iv) Solve for the pressure p on the wet interface.
(v) Recover the velocity V from step (i).
(vi) Calculate the radiated acoustic pressure at any field point by substituting V and p into the Helmholtz integral equation.

This solution sequence listed above solves structural FE equations of narrow band and full-populated fluid BE equations in two separate steps. The procedure adopted in this paper is:

(i) Solve, using potential decomposition technique, BE equations of the fluid to give the added mass matrix $[\tilde{\mathbf{m}}'_{rs}]$, damping matrix $[\tilde{\mathbf{n}}'_{rs}]$ and source distribution strength σ_{tj}. These terms will be defined carefully below.
(ii) Incorporate $[\tilde{\mathbf{m}}'_{rs}]$ and $[\tilde{\mathbf{n}}'_{rs}]$ into the structural mass matrix $[\mathbf{m}'_{rs}]$ and the damping matrix $[\mathbf{n}'_{rs}]$ to obtain the fluid-coupled structural dynamic equation.
(iii) Solve equation obtained in (ii) to give the displacement vector $\boldsymbol{\delta}$ at the structural nodes. The acoustic pressure at any field point can then be recovered from σ_{tj} and $\boldsymbol{\delta}$.

Although in this solution sequence the problem is divided into two separate matrix equations, the coupled structural dynamic equation is not a narrow band matrix equation. Consequently, it requires more computer memory than Everstine and Henderson's method. However, the solution

sequence presented in this paper has the advantage that it allows eigenvalue analysis to be performed on the fluid-loaded structure since the structural dynamic equation includes the effect of fluid loading. The key difficulty lies in the accurate computation of added mass and damping matrices due to fluid loading *before* the structural dynamic equations are solved. Most papers dealing with this problem are concerned with interior cavity or enclosure problems. For exterior domain problems, DeRunts and Geers [17] and Everstine [15,18] have computed added mass by solving Laplace's equation, whose solution is restricted to the low-frequency regime. Their approach is therefore only valid for incompressible fluids and does not include damping effects due to acoustic radiation. To compute acoustic added mass and damping coefficients for compressible fluids at arbitrary frequencies, the BE method discussed in Ref. [1] by the authors will be employed in this paper. The technique will be illustrated by computation of the sound pressure level (SPL) due to a ribbed cylindrical shell submerged in water. Validation of the method will be made by comparing the numerical results with experimental data by Chen and Schweikert [11].

2. Boundary element method for determining acoustic added mass and damping coefficients due to fluid loading

An uncoupled BE method and its validation has been described by the authors in Ref. [1] for determining added mass and damping coefficients due to fluid loading. The wet structural surface S_0 is discretized into N_{e0} elements. The spatial velocity potential ϕ, which is related to the time-dependent velocity potential Φ by $\Phi = \phi e^{i\omega t}$ (the time convention $e^{i\omega t}$ is assumed for consistency with that adopted in NASTRAN), can be decomposed as

$$\phi = i\omega \sum_{j=1}^{N_{e0}} \bar{W}_j \varphi_j, \tag{1}$$

where $\bar{W}_j$ is average displacement amplitude of element j, ω is the circular frequency and $i = \sqrt{-1}$. In Eq. (1) φ_j is the velocity potential due to the vibration of element j with unit-amplitude velocity, with all other elements kept stationary. Note that φ_j depends on frequency and the shape of the wetted surface, but is independent of the unknown displacement amplitude $\bar{W}_j$. Eq. (1) states that the total velocity potential ϕ at any point is the superposition of contributions of velocity potentials φ_j due to the vibration of jth element, where φ_j satisfies the differential equations [1]:

$$\nabla^2 \varphi_j + k^2 \varphi_j = 0, \tag{2a}$$

$$\lim_{r\to\infty} |r\varphi_j| < \infty, \tag{2b}$$

$$\lim_{r\to\infty} r\left(\frac{\varphi_j}{r} + ik\varphi_j\right) = 0, \tag{2c}$$

$$\left.\frac{\varphi_j}{n}\right|_{\mathbf{x}_r \in S_0} = \delta_{rj}. \tag{2d}$$

In the above, r is the distance between the field point and source point, ∇ is the Laplacian operator, $k = \omega/c_0$, c_0 is the sound speed, $\mathbf{n}$ unit outward normal from the wetted surface on the structure, δ_{rj} is the Kronecker delta function, and $\mathbf{x}_r$ indicates the rth field point. A solution of Eq. (2) at any point $\mathbf{x}$ can be expressed (see for example, Ref. [19, Eq. (1.76)]) as

$$\varphi_j(\mathbf{x}) = \iint_{S_0} \sigma_j(\mathbf{y}) G(\mathbf{x}, \mathbf{y}) \, \mathrm{d}S(\mathbf{y}), \tag{3}$$

where $\sigma_j = \sigma_j^c + \mathrm{i}\sigma_j^s$ (real and imaginary parts are indicated by superscripts c and s, respectively) is the unknown monopole source strength at the source point $\mathbf{y}$ on the wetted surface and $G(\mathbf{x}, \mathbf{y})$ is free space Green function [19]. In this paper, the Green function is further required to satisfy the boundary condition at the free water surface, which takes the form

$$G(\mathbf{x}, \mathbf{y}) = -\frac{1}{4\pi}\left(\frac{\mathrm{e}^{-\mathrm{i}kr}}{r} - \frac{\mathrm{e}^{-\mathrm{i}kr_1}}{r_1}\right), \tag{4}$$

where $r_1 = [(x_1 - y_1)^2 + (x_2 - y_2)^2 + (x_3 + y_3)^2]^{1/2}$; y_3 denotes the axis pointing upward to the free water surface. Since $G(\mathbf{x}, \mathbf{y})$ is the half-space Green function, Eq. (3) must satisfy Eqs. (2a)–(2c). To satisfy the wet interface boundary condition (2d), a Fredholm integral equation of the second kind must be solved, obtained by substituting Eq. (3) into Eq. (2d). The discrete form of this integral equation is the $2N_{e0}$ linear algebraic equations of BEM for the unknown source strength σ_{tj} ($t = 1, 2, 3, \ldots, N_{e0}$),

$$\sum_{t=1}^{N_{e0}} \begin{bmatrix} I_{rt}^c & -I_{rt}^s \\ I_{rt}^s & I_{rt}^c \end{bmatrix} \begin{Bmatrix} \sigma_{tj}^c \\ \sigma_{tj}^s \end{Bmatrix} = \begin{Bmatrix} \delta_{rj} \\ 0 \end{Bmatrix}, \quad j = 1, 2, 3, \ldots, N_{e0}, \tag{5}$$

where the subscript t denotes the element number. The terms I_{rt} represent influence coefficients of source strength, defined as

$$I_{rt} = I_{rt}^c + \mathrm{i}I_{rt}^s = (\mathbf{n}_r \cdot \nabla_{\mathbf{x}}) \iint_{S_t} G(\mathbf{x}, \mathbf{y}_t) \, \mathrm{d}S(\mathbf{y}_t)\big|_{\mathbf{x}=\mathbf{x}_r \in S_r}, \tag{6}$$

where S_r and S_t denote the rth and tth element facets on the wetted interface S_0, $\mathbf{n}_r$ is the outward unit normal vector of the element r, and $\nabla_{\mathbf{X}}$ denotes the differential operator $(\partial/\partial x_1)\mathbf{e}_1 + (\partial/\partial x_2)\mathbf{e}_2 + (\partial/\partial x_3)\mathbf{e}_3$, where $\mathbf{e}_i$ is the unit vector in x_i-direction. For $r = t$, the integral in Eq. (6) takes the principal value $I_{rt} = 0.5$. We assume that the element scale is about one tenth smaller than both the acoustic and the structural-bending wave length so that the source strength σ_{tj} on each element t can be taken as constant.

Eq. (5) represent a system of N_{e0} sets of algebraic equations ($j = 1, 2, 3, \ldots, N_{e0}$). However, since the coefficient matrix does not depend on j, only one matrix inverse needs to be performed.

The unsteady pressure in the fluid is related to the velocity potential by $p(\mathbf{x}, t) = -\rho_0 \partial\Phi/\partial t$, where ρ_0 is the mean density of the medium. Once the source strength distribution σ_{tj} on the wet interface is known, the pressure at any point $\mathbf{x}_k$ on the element facet S_k can be deduced from

Eqs. (1) and (3)

$$p(\mathbf{x}_k, t) = \sum_{j=1}^{N_{e0}} (-\bar{m}_{kj}\ddot{W}_j - \bar{n}_{kj}\dot{W}_j), \tag{7}$$

where $W_j = \bar{W}_j e^{i\omega t}$ is the normal displacement of element j, and $\dot{W}_j$ and $\ddot{W}_j$ are the normal velocity and acceleration of element j, respectively (for more explanations and derivation of Eq. (7), see Section 4 and note that $p = \bar{p}e^{i\omega t}$). Eq. (7) states that the pressure exerted on the kth element consists of two parts. One is directly proportional to the vibration acceleration of element j, its coefficient $\bar{m}_{kj}$ being referred to as the added mass. The other is directly proportional to the vibration velocity of element j, its coefficient $\bar{n}_{kj}$ being referred to as the damping coefficient. They can be calculated from

$$\bar{m}_{kj} = \rho_0 \sum_{t=1}^{N_{e0}} (A_{kt}^c \sigma_{tj}^c - A_{kt}^s \sigma_{tj}^s) \tag{8}$$

and

$$\bar{n}_{kj} = -\rho_0 \omega \sum_{t=1}^{N_{e0}} (A_{kt}^s \sigma_{tj}^c + A_{kt}^c \sigma_{tj}^s), \tag{9}$$

where A_{kt} is the velocity potential influence coefficient defined as

$$A_{kt}(\mathbf{x}_k) = A_{kt}^c + iA_{kt}^s = \iint_{S_t} G(\mathbf{x}_k, \mathbf{y}_t)\, dS(\mathbf{y}_t). \tag{10}$$

Thus, the coefficients $\bar{m}_{kj}$ and $\bar{n}_{kj}$ may be interpreted as the added mass and damping per unit area on the kth element due to vibration of the jth element. Although the pressure on the wet interface depends on the unknown structural variable W_j, the added mass $\bar{m}_{kj}$ and the damping coefficient $\bar{n}_{kj}$ are independent of W_j. Therefore, the method proposed in this paper is referred to as an *uncoupled* BEM.

3. Finite element dynamic equations of fluid-coupled structures

Before the FE dynamic equation can be assembled, the fluid loading terms of added mass and damping must be allocated to the structural nodes to form element matrices. These matrices, expressed in the local coordinate system, then need to be transferred to the FE global coordinate system [20].

The BE formulas given in the last section do not depend on the reference coordinate system since the distance r between source and field points is an invariant of any coordinate transformation. However, two coordinate systems are usually necessary for FE assembly since it is convenient to express element matrices in the local coordinates then transfer to the global coordinates. If $\mathbf{y}(y_1, y_2, y_3)$ and $\mathbf{y}'(y_1', y_2', y_3')$ refer to the local coordinate and global coordinate systems, respectively, the coordinate transformation can be implemented by $\mathbf{y} = \mathbf{t}\mathbf{y}'$ with $\mathbf{t}$ being a 3×3 matrix of direction cosines of angles formed between the two sets of axes. For a shell

structure, combined nodal displacements of plane stress and plate bending [20] in local and global coordinates can be written as

$$\boldsymbol{\delta} = \bar{\boldsymbol{\delta}}\, e^{i\omega t} = \{\, u \quad v \quad w \quad \theta_1 \quad \theta_2 \quad \theta_3 \,\}^{T}, \tag{11}$$

$$\boldsymbol{\delta}' = \bar{\boldsymbol{\delta}}'\, e^{i\omega t} = \{\, u' \quad v' \quad w' \quad \theta_1' \quad \theta_2' \quad \theta_3' \,\}^{T}, \tag{12}$$

where the superscript T indicates matrix transposition, the overbar indicates the amplitude of a time oscillating quantity, u, v, w correspond to translations in the direction of the three axes, and θ_1, θ_2, θ_3 refer to rotation angles around the three axes. The displacements of a particular node can be transformed from the global system to the local system by the matrix transformation

$$\boldsymbol{\delta} = \mathbf{T}\boldsymbol{\delta}', \tag{13}$$

where

$$\mathbf{T} = \begin{bmatrix} \mathbf{t} & 0 \\ 0 & \mathbf{t} \end{bmatrix}. \tag{14}$$

Since the plane stress displacement on the wet surface is generally not in the normal direction, only plate bending in the local coordinate system contributes to the fluid loading. If the shape function of the normal displacement w is assumed to be an incomplete cubic polynomial [20] in triangular area coordinates, the average amplitude of normal displacement of element j is given by

$$\bar{W}_j = \int\int_{S_j} \bar{w}_j \, dy_1 \, dy_2 / \Delta_j = \mathbf{D}_j \bar{\boldsymbol{\delta}}^b. \tag{15}$$

In Eq. (15) $\bar{w}_j$ is the amplitude of w, Δ_j is the area of the triangular element j, $\bar{\boldsymbol{\delta}}^b = \{\, \bar{\boldsymbol{\delta}}_l^b \quad \bar{\boldsymbol{\delta}}_m^b \quad \bar{\boldsymbol{\delta}}_n^b \,\}^{T}$, where $\bar{\boldsymbol{\delta}}_l^b = [\, \bar{w} \quad \bar{\theta}_1 \quad \bar{\theta}_2 \,]_l^{T}$ is the displacement amplitude of node l ($l \to m \to n$), superscripts b indicate the quantities related to plate bending, subscripts l, m, n indicate the node number of a triangular element, $\mathbf{D}_j = [\, \mathbf{d}_l \quad \mathbf{d}_m \quad \mathbf{d}_n \,]_j$, where $\mathbf{d}_l$ is calculated from

$$\mathbf{d}_l = \left[\, \tfrac{1}{3} \quad -\tfrac{1}{8} y_2 \quad \tfrac{1}{8} y_1 \,\right]_l \quad (l \to m \to n). \tag{16}$$

Substituting Eq. (15) into Eq. (7) and following a standard pattern of nodal allocation of distributed loading [20], a nodal equivalent added mass matrix, which relates the nodal forces to the corresponding nodal accelerations, is obtained of the form

$$[\tilde{\mathbf{m}}^b]_{kj} = \begin{bmatrix} \tilde{\mathbf{m}}_{ll}^b & \tilde{\mathbf{m}}_{lm}^b & \tilde{\mathbf{m}}_{ln}^b \\ \tilde{\mathbf{m}}_{ml}^b & \tilde{\mathbf{m}}_{mm}^b & \tilde{\mathbf{m}}_{mn}^b \\ \tilde{\mathbf{m}}_{nl}^b & \tilde{\mathbf{m}}_{nm}^b & \tilde{\mathbf{m}}_{nn}^b \end{bmatrix}_{kj} = \Delta_k \mathbf{D}_k^{T} r \bar{m}_{kj} \mathbf{D}_j \quad \text{for } k \neq j, \tag{17}$$

where each element of the matrix of Eq. (17) is a 3×3 sub-matrix of the form

$$[\tilde{\mathbf{m}}_{rs}^b]_{kj} = \Delta_k [\mathbf{d}_r]_k^{T} \bar{m}_{kj} [\mathbf{d}_s]_j \quad (r, s = l, m, n). \tag{18}$$

Eq. (18) may be interpreted as the added mass of the rth node on the kth element, caused by the acceleration of the sth node on element j; Δ_k is the area of triangular element k. Note that $[\tilde{\mathbf{m}}^b]_{kj}$ is

an asymmetric matrix since $[\mathbf{d}_r]_k \neq [\mathbf{d}_s]_j$. For the case of $j = k$, the matrix become

$$[\tilde{\mathbf{m}}^b]_{jj} = \bar{m}_{jj} \Delta_j [\mathbf{NN}]_j \quad \text{for } j = k, \tag{19}$$

where $[\mathbf{NN}]_j$ is a mass allocation matrix, details of which are given in the appendix.

Similarly a nodal equivalent damping matrix is given by

$$[\tilde{\mathbf{n}}^b]_{kj} = \begin{bmatrix} \tilde{\mathbf{n}}^b_{ll} & \tilde{\mathbf{n}}^b_{lm} & \tilde{\mathbf{n}}^b_{\ln} \\ \tilde{\mathbf{n}}^b_{ml} & \tilde{\mathbf{n}}^b_{mm} & \tilde{\mathbf{n}}^b_{mn} \\ \tilde{\mathbf{n}}^b_{nl} & \tilde{\mathbf{n}}^b_{nm} & \tilde{\mathbf{n}}^b_{nn} \end{bmatrix}_{kj} = \Delta_k \mathbf{D}_k^{\mathrm{T}} \bar{n}_{kj} \mathbf{D}_j \quad \text{for } k \neq j, \tag{20}$$

where

$$[\tilde{\mathbf{n}}^b_{rs}]_{kj} = \Delta_k [\mathbf{d}_r]_k^{\mathrm{T}} \bar{\mathrm{n}}_{kj} [\mathbf{d}_s]_j \quad (r, s = l, m, n). \tag{21}$$

For $j = k$

$$[\mathbf{n}^b]_{jj} = \bar{n}_{jj} \Delta_j [\mathbf{NN}]_j. \tag{22}$$

The added mass and damping matrices due to combined plane stress and plate bending, can be written as

$$[\tilde{\mathbf{m}}_{rs}]_{kj} = \begin{bmatrix} 0 & 0 & 0 & 0 & 0 & 0 \\ 0 & 0 & 0 & 0 & 0 & 0 \\ 0 & 0 & & & & 0 \\ 0 & 0 & & [\tilde{\mathbf{m}}^b_{rs}]_{kj} & & 0 \\ 0 & 0 & & & & 0 \\ 0 & 0 & 0 & 0 & 0 & 0 \end{bmatrix}, \quad [\tilde{\mathbf{n}}_{rs}]_{kj} = \begin{bmatrix} 0 & 0 & 0 & 0 & 0 & 0 \\ 0 & 0 & 0 & 0 & 0 & 0 \\ 0 & 0 & & & & 0 \\ 0 & 0 & & [\tilde{\mathbf{n}}^b_{rs}]_{kj} & & 0 \\ 0 & 0 & & & & 0 \\ 0 & 0 & 0 & 0 & 0 & 0 \end{bmatrix}. \tag{23}$$

In the global coordinate system, the added mass and damping matrices, which are caused by vibration of the sth node of element j, of the rth node of element k are

$$[\tilde{\mathbf{m}}'_{rs}]_{kj} = [\mathbf{T}]_k^{\mathrm{T}} [\tilde{\mathbf{m}}_{rs}]_{kj} [\mathbf{T}]_j, \tag{24}$$

$$[\tilde{\mathbf{n}}'_{rs}]_{kj} = [\mathbf{T}]_k^{\mathrm{T}} [\tilde{\mathbf{n}}_{rs}]_{kj} [\mathbf{T}]_j, \tag{25}$$

where $\mathbf{T}$ is the coordinate transformation matrix given by Eq. (14), and the use of the prime indicate a quantity expressed in global coordinates. Assembled added mass and damping matrices in the global coordinate system can be obtained from element matrices of Eqs. (24) and (25) as

$$[\tilde{\mathbf{m}}'_{rs}] = \sum_k \sum_j [\tilde{\mathbf{m}}'_{rs}]_{kj}, \tag{26}$$

$$[\tilde{\mathbf{n}}'_{rs}] = \sum_k \sum_j [\tilde{\mathbf{n}}'_{rs}]_{kj}, \tag{27}$$

where $\sum_k$ indicates summation with respect to all the elements k which are related to node r, and $\sum_j$ indicates summation with respect to all the elements j which are related to node s.

Since transformation matrices $\mathbf{T}$ vary from element to element (e.g. $[\mathbf{T}]_k \neq [\mathbf{T}]_j$), $[\tilde{\mathbf{m}}'_{rs}]$ and $[\tilde{\mathbf{n}}'_{rs}]$ are generally asymmetric. Therefore, the assembled added mass and damping matrices of Eqs. (26) and (27) are asymmetric and frequency dependent (see Eqs. (8) and (9)).

Define

$$\begin{aligned} \mathbf{C}^c_{rs} &= -\omega^2(\mathbf{m}'_{rs} + \tilde{\mathbf{m}}'_{rs}) + \mathbf{K}'_{rs}, \\ \mathbf{C}^s_{rs} &= \omega(\mathbf{n}'_{rs} + \tilde{\mathbf{n}}'_{rs}), \end{aligned} \tag{28}$$

where $\left[\mathbf{K}'_{rs}\right]$, $[\mathbf{m}'_{rs}]$ and $[\mathbf{n}'_{rs}]$ are, respectively, global stiffness, mass and damping matrices of the structure. One should note that $\tilde{\mathbf{m}}'_{rs}$ and $\tilde{\mathbf{n}}'_{rs}$ are taken to equal zero for any node r or s that is not located on the wet structural surface since the acoustic pressure is assumed to propagate only through the dense fluid. The fluid-coupled FE dynamic equation can now be written as

$$\sum_{s=1}^{N_p} \begin{bmatrix} \mathbf{C}^c_{rs} & -\mathbf{C}^s_{rs} \\ \mathbf{C}^s_{rs} & \mathbf{C}^c_{rs} \end{bmatrix} \begin{Bmatrix} \bar{\boldsymbol{\delta}}'^c_s \\ \bar{\boldsymbol{\delta}}'^s_s \end{Bmatrix} = \begin{Bmatrix} \bar{\mathbf{F}}'^c_r \\ \bar{\mathbf{F}}'^s_r \end{Bmatrix}, \quad r = 1, 2, 3, \ldots, N_p, \tag{29}$$

where $\{\bar{\boldsymbol{\delta}}'_s\} = \{\bar{\boldsymbol{\delta}}'^c_s\} + \mathrm{i}\{\bar{\boldsymbol{\delta}}'^s_s\}$ is the vector of nodal displacement amplitudes, $\{\bar{\mathbf{F}}'_r\} = \{\bar{\mathbf{F}}'^c_r\} + \mathrm{i}\{\bar{\mathbf{F}}'^s_r\}$ is the vector of nodal force amplitudes, and N_p is the number of nodes. Thus, we require the solution to $12 \times N_p$ algebraic equations and unknown nodal displacements (including the real and imaginary parts).

4. Calculation of acoustic pressure

The solution of the fluid-coupled FE Eq. (29) gives the nodal displacement amplitudes $\{\bar{\boldsymbol{\delta}}'_s\}$. Once this solution is obtained, the average amplitude $\bar{W}_j = \bar{W}^c_j + \mathrm{i}\bar{W}^s_j$ of the normal displacements of the element j on the wet surface can be calculated by substituting $\{\bar{\boldsymbol{\delta}}'_s\}$ into Eqs. (13) and (15). The acoustic pressure $\bar{p}(\mathbf{x}_k) = \bar{p}^c(\mathbf{x}_k) + \mathrm{i}\bar{p}^s(\mathbf{x}_k)$ at any field point $\mathbf{x}_k$ can then be determined from the relation $p(\mathbf{x}, t) = -\rho_0 \partial\Phi/\partial t$ and Eqs. (1) and (3)

$$\bar{p}^c(\mathbf{x}_k) = \rho_0\omega^2 \sum_{j=1}^{N_{e0}} (\varphi^c_j(\mathbf{x}_k)\bar{W}^c_j - \varphi^s_j(\mathbf{x}_k)\bar{W}^s_j), \tag{30}$$

$$\bar{p}^s(\mathbf{x}_k) = \rho_0\omega^2 \sum_{j=1}^{N_{e0}} (\varphi^s_j(\mathbf{x}_k)\bar{W}^c_j + \varphi^c_j(\mathbf{x}_k)\bar{W}^s_j), \tag{31}$$

where the velocity potential φ_j is given by

$$\varphi_j(\mathbf{x}_k) = \varphi^c_j(\mathbf{x}_k) + \mathrm{i}\varphi^s_j(\mathbf{x}_k) = \sum_{t=1}^{N_{e0}} \left[(A^c_{kt}\sigma^c_{tj} - A^s_{kt}\sigma^s_{tj}) + \mathrm{i}(A^s_{kt}\sigma^c_{tj} + A^c_{kt}\sigma^s_{tj}) \right]. \tag{32}$$

5. Numerical results and validation of the method

The procedure described above for calculation of the dynamic response of fluid loaded structures may be summarized thus:

(i) Generate structural FE mesh and ensure that BE share the same mesh with FE on the wet interface.
(ii) Calculate coefficient I_{rt} from Eq. (6), solve Eq. (5) to obtain source distribution σ_{tj}, then calculate the added mass $\bar{m}_{kj}$ and damping coefficient $\bar{n}_{kj}$ due to fluid loading from Eqs. (8) and (9).
(iii) Calculate the assembled added mass matrix $[\tilde{\mathbf{m}}'_{rs}]$ and damping matrix $[\tilde{\mathbf{n}}'_{rs}]$ from Eqs. (26) and (27), add them to the structural mass matrix $[\mathbf{m}'_{rs}]$ and damping matrix $[\mathbf{n}'_{rs}]$ through the DMAP module in NASTRAN.
(iv) Use NASTRAN to solve fluid-coupled FE dynamic equation (29) and output $\{\tilde{\boldsymbol{\delta}}_s\}$ through DMAP, or to extract eigenvalues for the fluid-coupled structure.
(v) Calculate $\bar{W}_j$ from Eq. (15), then obtain the acoustic pressure from Eqs. (30) and (31).

A numerical example of the method and its application to calculating the added mass and damping due to fluid loading has been discussed in Ref. [1]. Here we focus on the calculation of the vibration response and its acoustic radiation.

5.1. Forced vibration of a ribbed cylindrical shell

The vibration response and the sound pressure radiated by an underwater ribbed cylindrical shell will be calculated and the SPL will be compared with the experimental data of Chen and Schweikert [11]. Fig. 1 shows the dimensions of the steel shell and the experimental installation. Details of the experiment can be found in Ref. [11]. The excitation force, $F = \cos(2\pi ft)$ pounds,

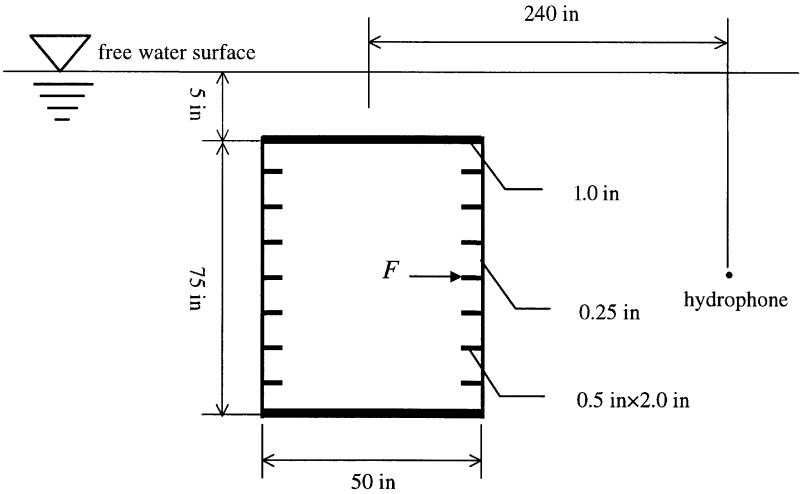

Fig. 1. Dimension of a ribbed cylindrical shell and experimental installation.

with frequency $f = 258\,\text{Hz}$ is applied to a point on the middle rib, as shown in Fig. 1. The structure is assumed to have a Youngs' modulus of $E = 2.06 \times 10^6\,\text{kg/cm}^2$, a Poisson's ratio of $v = 0.3$ and a structural damping ratio of $2\varsigma = 0.06$. The sound speed in the surrounding fluid is assumed to be $c_0 = 1461.0\,\text{m/s}$.

The shell is meshed into 1714 elements and 987 nodes with 1476 wet elements and 740 wet node on the wet interface, as shown in Fig. 2. Fig. 3 depicts the acoustic field mesh for which the radiated SPL at the nodal points will be calculated in order to obtain an acoustic contour map as shown in Fig. 6b. The acoustic field mesh is located in the horizontal plane midway along the cylinder length with sector radius ranging from 0.7 to 10.5 m. The BE mesh, which is same as the

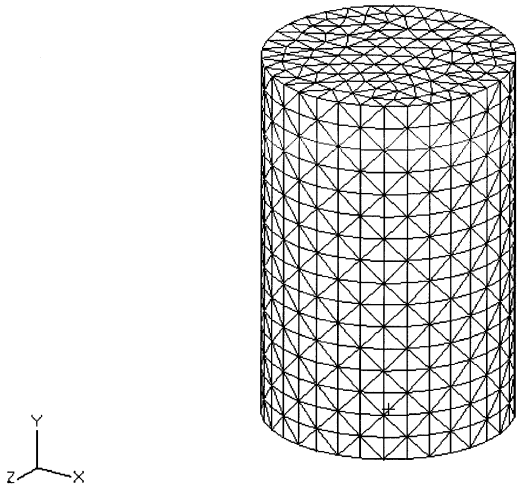

Fig. 2. Finite element mesh.

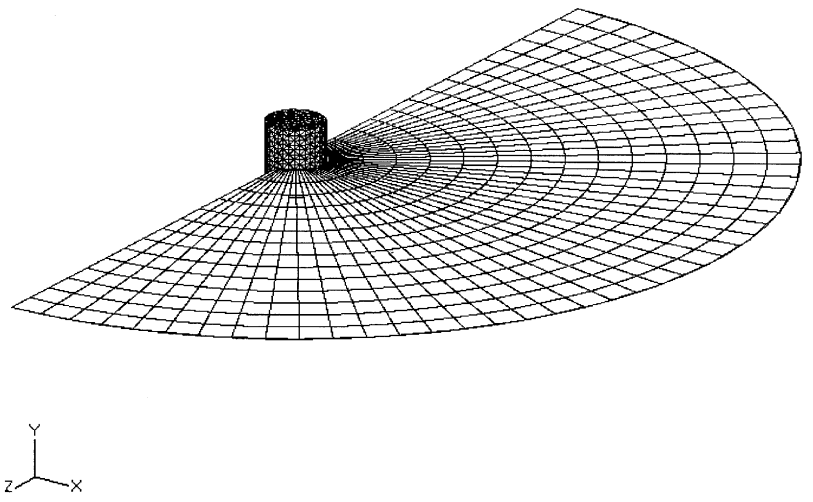

Fig. 3. BE mesh and acoustic field mesh.

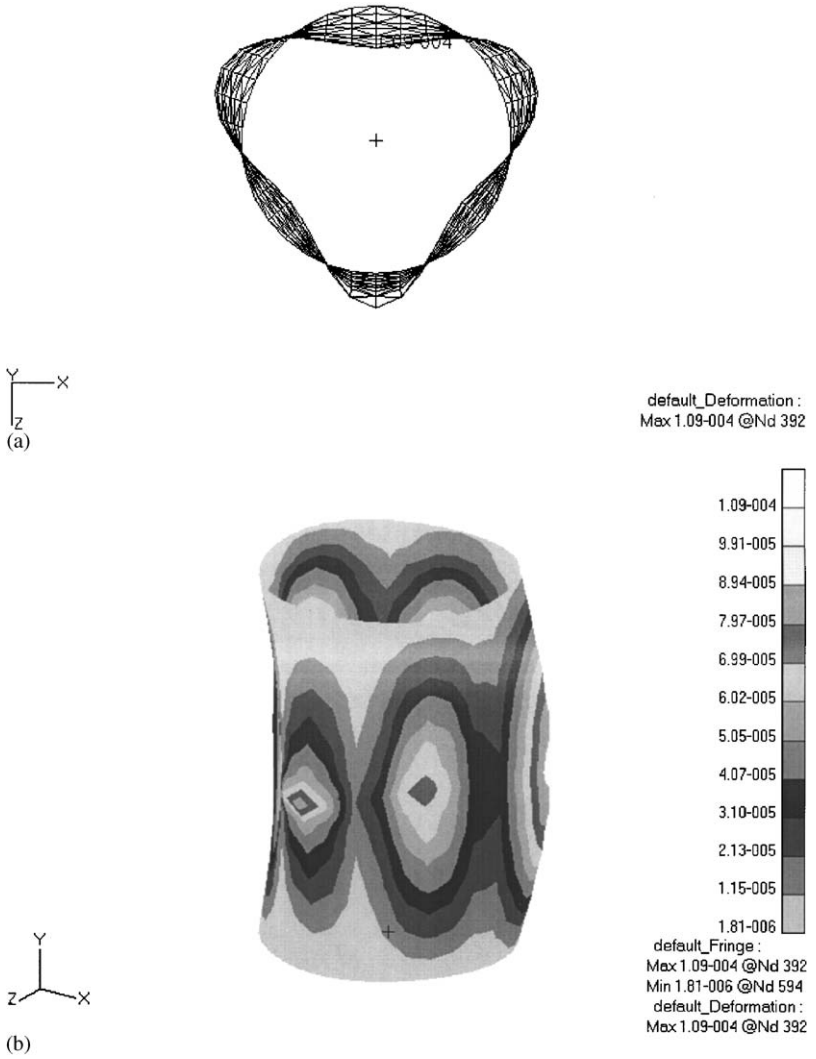

Fig. 4. (a) Deformation in vacuum; (b) contour map of deformation in vacuum.

FE mesh on the wet interface, is also show in Fig. 3, so that the relative position of the acoustic mesh can be seen.

Fig. 4 shows the displacement response of the forced vibration in a vacuum for the excition force described above. Fig. 5 is the corresponding response in water for the same excition force as in Fig. 4. Both are calculated using the NASTRAN solution sequence SOL108 (i.e., the direct frequency response method). Figs. 4a and 5a are the displacement deformations as viewed downwards onto the cylinder. Figs. 4b and 5b are the contour maps of displacement deformations, where the grey-scale level relates to the magnitude of vibration. In these figures, the upper and lower ends of the cylindrical shell are removed to allow a clearer view.

It can be seen that the vibration response in vacuum differs significantly from that in water. The maximum displacement amplitude in vacuum is 1.09×10^{-4} mm while it is 4.04×10^{-5} mm in

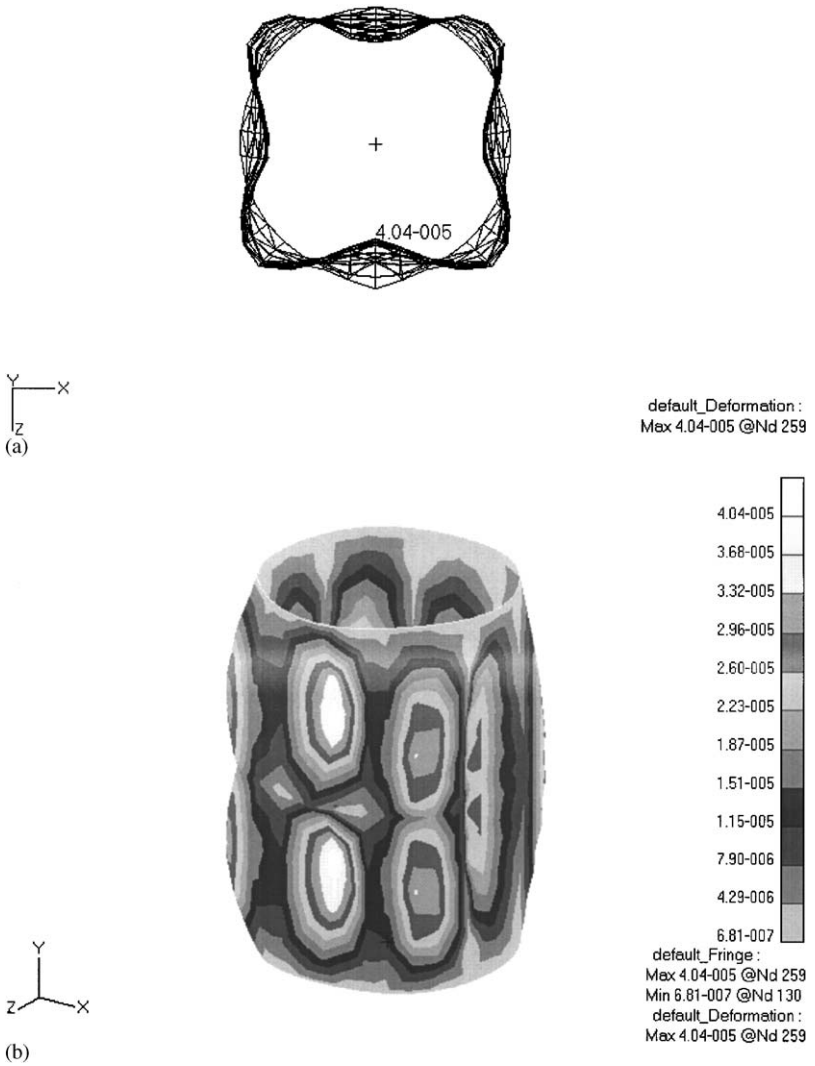

Fig. 5. (a) Deformation in water; (b) contour map of deformation in water.

water. Note that the computation time required for the above calculation in water is about 298 minutes on an Intel Pentium III, 1.1 GHz computer (approximately half of this time is spent on the calculation of added mass and damping) while in a vacuum it is less than 1 min. The main difference in solving coupled problems is the extra computation involved in the hydrodynamic calculation and in solving the matrix of coupled dynamic equations, which is non-narrow band unlike when fluid loading can be neglected.

Fig. 6a is a comparison between numerical results and experimental data. The polar axis indicates the SPL in dB (Ref. 1.0 μPa). The polar angles correspond to the angle of the field points of measurement. The measurement and calculation points are located at a radius of 240 in as shown in Fig. 1. The solid line in Fig. 6a is plotted from Chen and Schweikert's experimental data

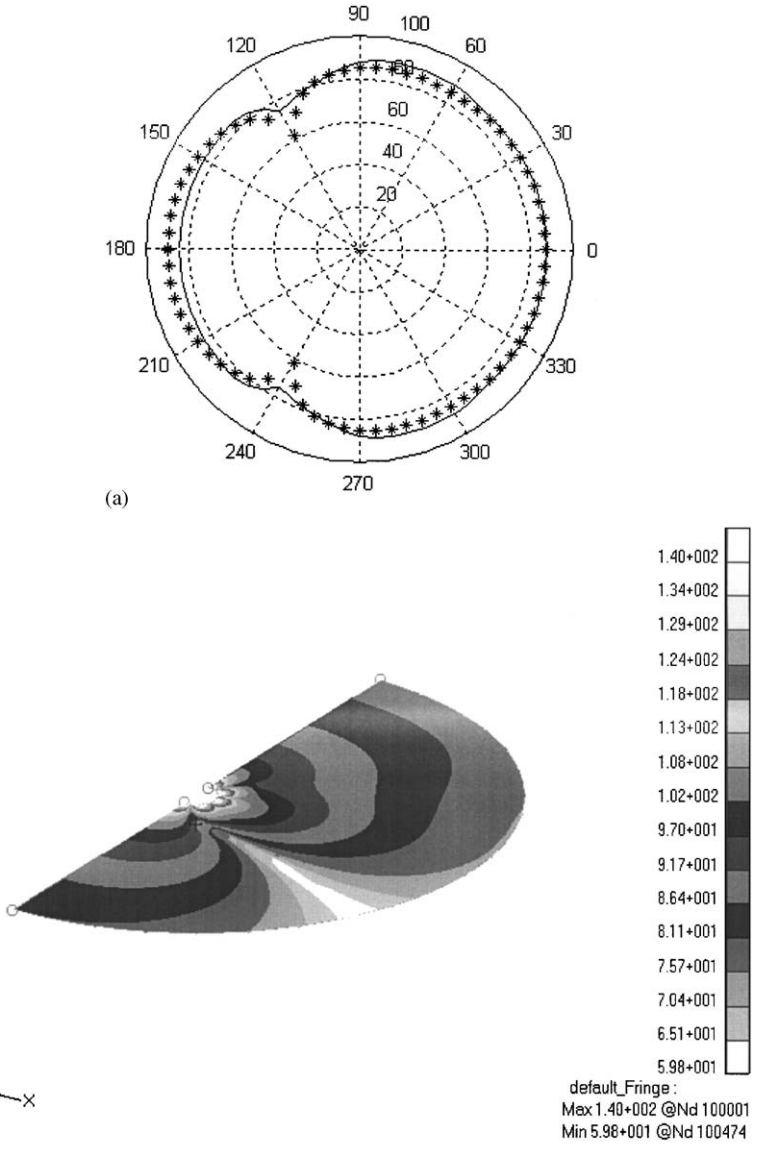

Fig. 6. (a) Comparison between numerical SPL and experimental data; (b) contour map of radiated SPL.

[11] and the points represented by stars denote the numerical results. The numerical results include the effect of reflections from the free water surface. The error between numerical results and the experimental data are less than 4 dB, except at the minimum SPL points where the experimental data may be in error due to low signal-to-noise ratio. Fig. 6b shows the contour map of SPL at the corresponding nodes (field points) of the acoustic mesh. The grey-scale level indicates the SPL in dB. The predicted directivity of the sound field has the same lobe structure as the experiment data at a distance slightly farther from the shell.

5.2. Eigenvalue analysis of the ribbed cylindrical shell

The ribbed cylindrical shell described in Section 5.1 will be used here for eigenvalue analysis of the fluid-coupled structure. Eigenvalue analysis of underwater structures is difficult for two main reasons. First the mass matrix of fluid-coupled structure is asymmetric, and therefore a complex eigenvalue solver is needed to extract the eigenvalues. Second, the added mass and damping of fluid are frequency dependent (see Eqs. (8) and (9)), which are unknown before the eigenvalue problem is solved. An iterative method must therefore be employed to determine the natural frequencies. The procedure of the iterative method is summarized as follows:

(i) Select several acoustic frequencies f_a (which are the frequencies used to calculate the added mass and damping due to fluid loading) to calculate the added mass and damping due to fluid loading
(ii) For each acoustic frequency f_a, use the complex eigenvalue solution sequence SOL107 of NASTRAN to solve the mode frequency f_m of an individual mode
(iii) Plot the mode frequency f_m against the acoustic frequency f_a, shown as a solid line marked with '*' in Fig. 7
(iv) Draw the equi-frequency line $f_m = f_a$, shown as a solid line in Fig. 7. The actual mode frequency of the ribbed cylindrical shell can be identified at the point of intersection of the two curves. In this example it is $f_m = 136.3$ Hz.

Table 1 presents a comparison between mode frequencies of the ribbed cylindrical shell in vacuum and in water. The mode frequencies in vacuum are calculated by using the real eigenvalue

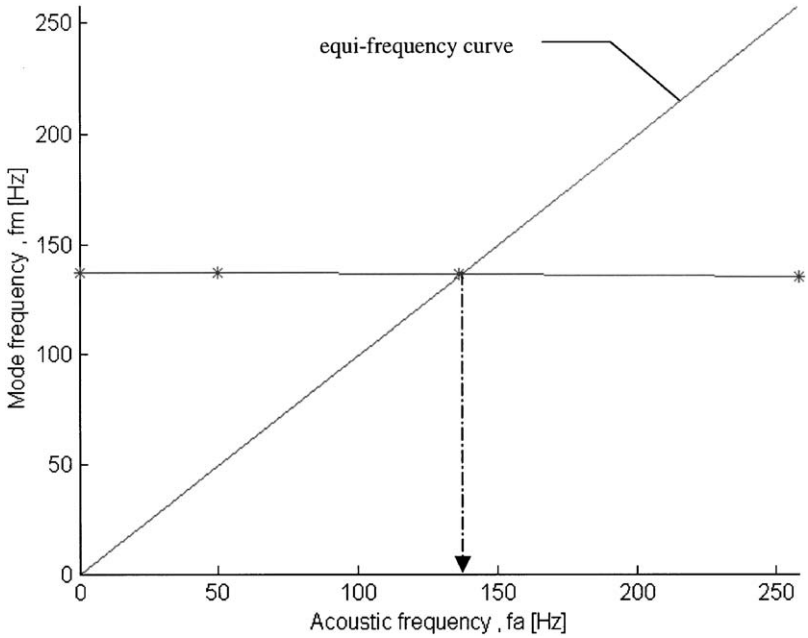

Fig. 7. Relation between mode and acoustic frequencies.

Table 1
Comparison of mode frequencies

Mode character		Mode of two circumferential lobes	Mode of three circumferential lobes	Mode of three circumferential and two vertical lobes	Mode of four circumferential lobes	Mode of two circumferential and two vertical lobes	Mode of four circumferential and two vertical lobes
Mode frequencies f_m (Hz) in vacuum		218.22	262.05	404.40	456.26	507.23	509.96
Mode frequencies f_m (Hz) in water for different acoustic frequencies f_a (Hz)	$f_a = 0.0$	106.59	137.13	222.60	252.74	265.51	291.63
	$f_a = 50.0$	106.48	137.06	222.54	252.68	265.36	291.57
	$f_a = 136.0$	105.69	136.64	222.08	252.28	264.41	291.21
	$f_a = 258.0$	102.93	135.29	220.69	251.02	261.34	290.11

solution sequence SOL103 of NASTRAN while the mode frequencies in water are extracted by using the complex eigenvalue solution sequence SOL107 of NASTRAN. The mode frequencies f_m in water are not the mode frequencies obtained by the iterative method given above, but the mode frequencies f_m for which the added mass and damping coefficient due to fluid loading are calculated at a given acoustic frequency f_a (note that f_a and f_m are not equal except once the iterative procedure is followed and the solution has converged). From Table 1 the invacuo mode frequencies are about two-times larger than the underwater mode frequencies for the same mode.

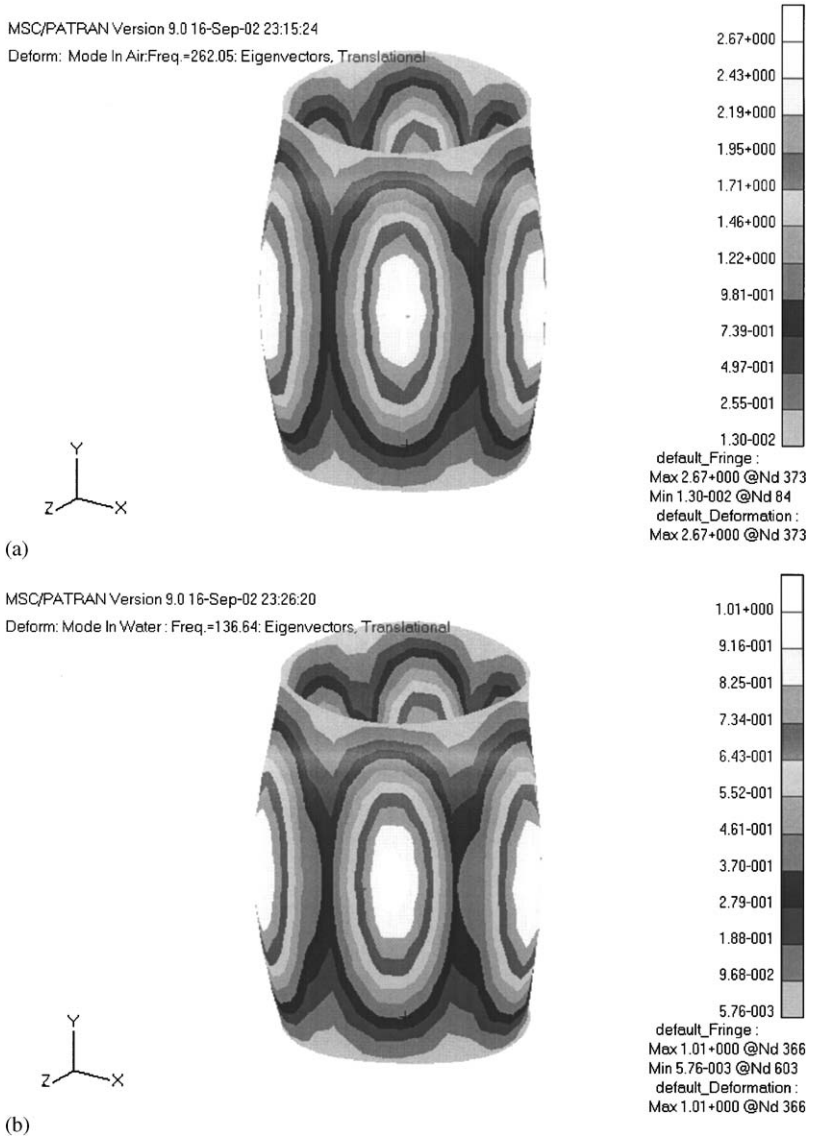

Fig. 8. (a) Mode shape of three circumferential lobes in vacuum, $f_m = 262.05$ Hz; (b) mode shape of three circumferential lobes in water, $f_m = 136.64$ Hz.

The results of Table 1 suggest that the structural mode frequency is not sensitive to the acoustic frequency if the acoustic wavelength is about twice as large as the maximum structural dimension. However, the mode frequencies are dramatically changed when the acoustic wavelengths are comparable with the structural scale. Further work is needed in order to establish definitive criteria. For large-scale structures at high frequencies, a finer mesh is required. Therefore, the FE dynamic matrix will be larger and the mode density of the structure is higher. In this case statistical energy analysis [21] may be a more appropriate method.

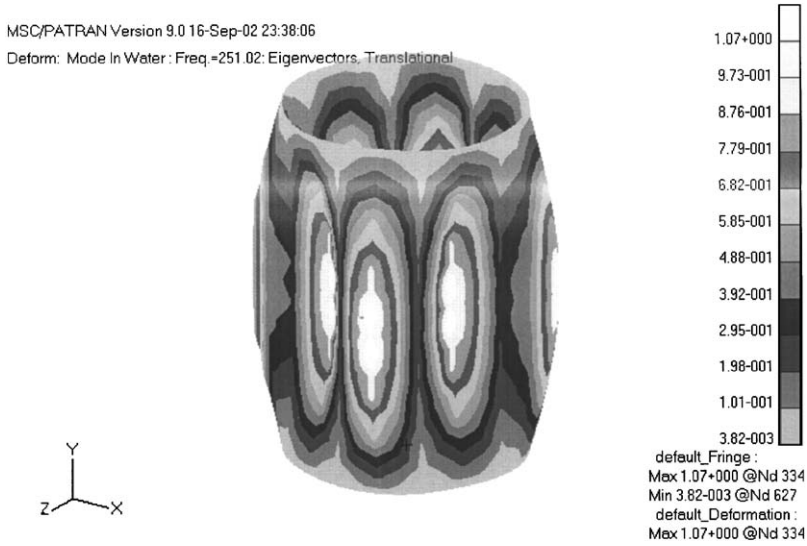

Fig. 9. Mode shape of four circumferential lobes in water, $f_m = 251.02\,\text{Hz}$.

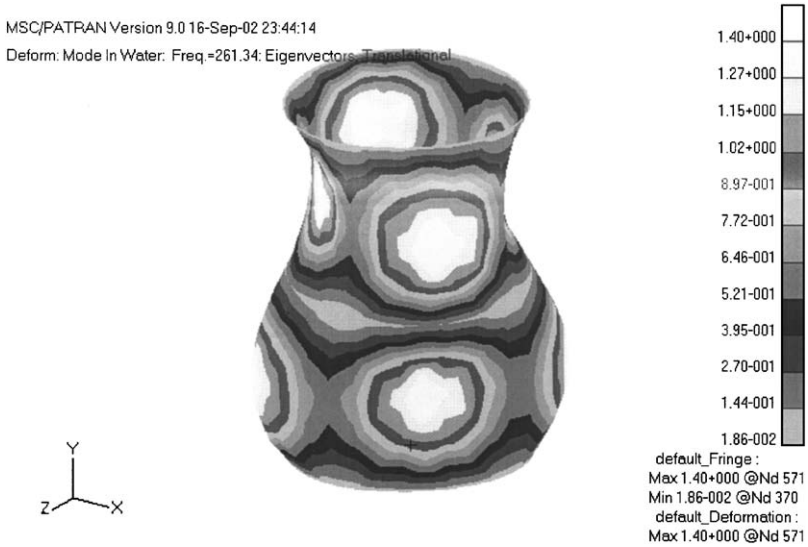

Fig. 10. Mode shape of two circumferential and two vertical lobes in water, $f_m = 261.34\,\text{Hz}$.

Figs. 8(a) and (b) are contour maps of mode shape of three circumferential lobes in vacuum and in water. The corresponding mode frequencies are $f_m = 262.05$ and 136.64 Hz. Although the difference between the two frequencies is large, the mode shapes are very similar. Fig. 9 is the mode shape corresponding to four circumferential lobes in water with natural frequency $f_m =$ 251.02 Hz. Fig. 10 is the mode shape corresponding to two circumferential and two vertical lobes in water with natural frequency $f_m = 261.34$ Hz. It can be seen from Fig. 5b that the forced vibration of the submerged shell mainly comprises the two mode shapes shown above.

6. Conclusion

An approach combining finite element and boundary element methods is proposed to calculate the elastic vibration and acoustic radiation from an underwater structure. The FEM software NASTRAN is employed for structural computation. An uncoupled boundary element method, based on the potential decomposition technique, is used to determine the acoustic added mass and damping coefficients. The acoustic matrices of added mass and damping coefficients are then added to the structural mass and damping matrices, respectively, by the use of DMAP modules in NASTRAN. The numerical results are shown to be in good agreement with experimental data. Furthermore, the complex eigenvalue of underwater structure are obtained by the NASTRAN solution sequence SOL107. This work suggests that the mode frequencies of underwater structures are only weakly dependent on the acoustic frequency if the acoustic wavelength is about twice as large as the maximum structural dimension.

Appendix A. Mass allocation matrix

The mass allocation matrix of element j is defined as

$$[\mathbf{NN}]_j = \frac{1}{\Delta_j}\iint_{S_j} \mathbf{N}^{\mathrm{T}}\mathbf{N}\,\mathrm{d}y_1\,\mathrm{d}y_2 = \begin{bmatrix} \mathbf{NN}^b_{ll} & \mathbf{NN}^b_{lm} & \mathbf{NN}^b_{\mathrm{ln}} \\ \mathbf{NN}^b_{ml} & \mathbf{NN}^b_{mm} & \mathbf{NN}^b_{mn} \\ \mathbf{NN}^b_{nl} & \mathbf{NN}^b_{nm} & \mathbf{NN}^b_{nn} \end{bmatrix}, \tag{A.1}$$

where $\mathbf{N}$ is shape function of plate bending displacement. If the shape function of normal displacement w is assumed to be an incomplete cubic polynomial [20] in triangular area coordinates, the 3×3 sub-matrix $\mathbf{NN}^b_{rs}\,(r, s = l, m, n)$ can be calculated as follow. For $r = s$,

$$[\mathbf{NN}^b_{ll}] = \begin{bmatrix} \frac{121}{630} & \frac{13}{630}(b_m - b_n) & \frac{13}{630}(c_m - c_n) \\ \frac{13}{630}(b_m - b_n) & \frac{1}{10080}(31b_m^2 + 31b_n^2 - 38b_m b_n) & \frac{1}{10080}(31b_m c_n + 31b_n c_n - 19b_n c_m - 19b_m c_n) \\ & & \frac{13}{630}(c_m - c_n) \\ & & \frac{1}{10080}(31b_m c_m + 31b_n c_n - 19b_n c_m - 19b_m c_n) \\ & & \frac{1}{10080}(31c_m^2 + 31c_n^2 - 38c_m c_n) \end{bmatrix}, \tag{A.2}$$

for $r = l$, $s = m$; $r = m$, $s = n$,

$$[\mathbf{NN}^b_{lm}] = \begin{bmatrix} \frac{89}{1260} & \frac{1}{2520}(34b_n - 19b_l) & \frac{1}{2520}(34c_n - 19c_l) \\ \frac{1}{2520}(19b_m - 34b_n) & \frac{1}{10080}(13b_m b_n + 13b_n b_l - 11b_m b_l - 25b_n^2) & \frac{1}{10080}(13b_m c_n + 13b_n c_l - 11b_m c_l - 25b_n c_n) \\ \frac{1}{2520}(19c_m - 34c_n) & \frac{1}{10080}(13b_n c_m + 13b_l c_n - 11b_l c_m - 25b_n c_n) & \frac{1}{10080}(13c_m c_n + 13c_n c_l - 11c_m c_l - 25c_n^2) \end{bmatrix}, \tag{A.3}$$

for $r = l$, $s = n$,

$$[\mathbf{NN}^b_{\ln}] = \begin{bmatrix} \frac{89}{1260} & \frac{1}{2520}(19b_l - 34b_m) & \frac{1}{2520}(19c_l - 34c_m) \\ \frac{1}{2520}(34b_m - 19b_n) & \frac{1}{10080}(13b_l b_m + 13b_m b_n - 11b_l b_n - 25b_m^2) & \frac{1}{10080}(13b_m c_l + 13b_n c_m - 11b_n c_l - 25b_m c_m) \\ \frac{1}{2520}(34c_m - 19c_n) & \frac{1}{10080}(13b_l c_m + 13b_m c_n - 11b_l b_n - 25b_m c_m) & \frac{1}{10080}(13c_l c_m + 13c_m c_n - 11c_l c_n - 25c_m^2) \end{bmatrix}, \tag{A.4}$$

where b_m, c_m can be calculated from local nodal coordinates

$$b_l = y_2^m - y_2^n, \quad c_l = y_1^n - y_1^m. \tag{A.5}$$

The subscripts or superscripts l, m, n of Eqs. (A.2)–(A.5) are local node numbers of triangle element with cyclic permutation of indices ($l \to m \to n \to l$). $[\mathbf{NN}^b_{rs}]$ is symmetric matrix, e.g. $\left[\mathbf{NN}^b_{sr}\right] = \left[\mathbf{NN}^b_{rs}\right]^{\mathrm{T}}$.

References

[1] Q. Zhou, W. Zhang, P.F. Joseph, A new method for determining acoustic added mass and damping coefficients of fluid–structure interaction, in: Y.S. Wu, et al. (Eds.), *The Eighth International Symposium on Practical Design of Ships and Other Floating Structures*, Elsevier, Amsterdam, 2001, pp. 1185–1195.

[2] A. Ali, C. Rajakumar, S.M. Yunus, Advances in acoustic eigeinvalue analysis using boundary element method, *Computers and Structures* 56 (1995) 834–847.

[3] L. Kiefling, G.C. Feng, Fluid–structure finite element vibrational analysis, *AIAA Journal* 14 (1976) 199–203.

[4] O.C. Zienkiewicz, P. Bettess, Fluid–structure dynamic interaction and wave forces: an introduction to numerical treatment, *International Journal for Numerical Methods in Engineering* 13 (1978) 1–6.

[5] H.C. Chen, R.L. Taylor, Vibration analysis of fluid–solid systems using a finite element displacement formulation, *International Journal for Numerical Methods in Engineering* 29 (1981) 683–698.

[6] G.G. Everstine, A symmetric Potential formulation for fluid–structure interaction, *Journal of Sound and Vibration* 79 (1981) 157–160.

[7] P. Bettess, Infinite elements, *International Journal for Numerical Methods in Engineering* 11 (1977) 53–64.

[8] O.C. Zienkiewicz, K. Bando, P. Bettess, T.C. Chiam, Mapped infinite elements for exterior wave problems, *International Journal for Numerical Methods in Engineering* 21 (1985) 1229–1251.

[9] E.T. Moyer Jr., Performance of mapped infinite elements for exterior wave scattering applications, *Communications in Applied Numerical Methods* 8 (1992) 27–39.
[10] R.J. Astley, Infinite elements for wave problems: a review of current formulations and an assessment of accuracy, *International Journal for Numerical Methods in Engineering* 49 (2000) 951–976.
[11] L.H. Chen, D.G. Schweikert, Sound radiation from an arbitrary body, *Journal of the Acoustical Society of America* 35 (1963) 1626–1632.
[12] A.F. Seybert, T.W. Wu, X.F. Wu, Radiation and scattering of acoustic waves from elastic solids and shells using the boundary element method, *Journal of the Acoustical Society of America* 84 (1988) 1906–1912.
[13] G.C. Everstine, F.M. Henderson, Coupled finite element/boundary element approach for fluid–structure interaction, *Journal of the Acoustical Society of America* 87 (1990) 1938–1947.
[14] P.M. Pinsky, N.N. Abboud, Transient finite element analysis of the exterior structural acoustics problem, in: R.J. Bernhard, R.F. Keltie (Eds.), *Numerical Techniques in Acoustic Radiation*, NCA-Vol. 6, American Society of Mechanical Engineers, New York, 1989, pp. 35–47.
[15] G.C. Everstine, Finite element formulations of structural acoustics problem, *Computers and Structures* 65 (3) (1997) 307–321.
[16] L. Morino, Boundary integral equations in aerodynamics, *Applied Mechanical Review* 46 (1993) 445–466.
[17] J.A. DeRunts, T.L. Geers, Added mass computation by the boundary element method, *International Journal for Numerical Methods in Engineering* 12 (1978) 531–549.
[18] G.C. Everstine, Prediction of low frequency vibrational frequencies of submerged structures, *Journal of Vibration and Acoustics* 113 (1991) 187–191.
[19] M.E. Goldstein, *Aeroacoustics*, McGraw-Hill, New York, 1976.
[20] O.C. Zienkiewicz, R.L. Taylor, *The Finite Element Method*, fourth ed., McGraw-Hill, New York, 1991.
[21] R.H. Lyon, R.G. DeJong, *The Theory and Application of Statistical Energy Analysis*, second ed., Butterworth-Heinemann, London, 1995.